Engineering Journal issn: 0125-8281

Article

A 3D End-Effector Robot for Upper Limb Functional Rehabilitation of Hemiparesis Patients

Kewalee Asawapithulsert[1,a], Anan Sutapun[2,b], Maitai Dahlan[1], and Viboon Sangveraphunsiri[3,c,*]

1 Department of Mechanical Engineering, Faculty of Engineering, Chulalongkorn University, 254 Phayathai Rd., Pathumwan, Bangkok 10330, Thailand
2 Haxter Robotics, Bangkok 10330, Thailand
3 Faculty of Engineering, Chulalongkorn University, Bangkok 10330, Thailand
E-mail: [a]kewalee.asa@gmail.com, [b]anansutapun@gmail.com,
[c,*]viboon.s@chula.ac.th (Corresponding author)

Abstract. Robot-assisted therapy is a new type of rehabilitation that allows for highly repetitive, intensive, adaptable, and quantifiable physical training. It is increasingly being used to restore motor function, particularly in stroke survivors with upper limb paresis. The end-effector type robot allows natural movements without complex structure which is ideal for functional rehabilitation training. A 3D end-effector base on a five-bar linkage has been proposed to improve the common end-effector type that covers mechanical design, dynamic control strategy, and application of rehabilitation training or exercise. The dynamic controllers are deweighting with gravity compensation, passive mobilization or active assistive, and the virtual spring-damper wall concept. These controllers are used for developing functional rehabilitation training or exercise from an engineering point of view based on experiences in developing various types of rehabilitation robots. The experiments, based on the performance of the controllers, have been conducted with healthy subjects. The experimental results have shown very promising results and can be extended to various types of functional rehabilitation.

Keywords: Virtual wall strategy, robot-assisted therapy, hemiparesis, rehabilitation robot, the 3D end-effector robot.

ENGINEERING JOURNAL Volume 26 Issue 11
Received 22 June 2022
Accepted 21 November 2022
Published 30 November 2022
Online at https://engj.org/
DOI:10.4186/ej.2022.26.11.29

DOI:10.4186/ej.2022.26.11.29

1. Introduction

Stroke is the leading cause of paralysis and the most common health issue, according to the 2016 Global Neurological DALYs Index. Especially the elderly (around 60 to 80 years old) who have the highest impact, even though stroke prevention and treatment technology have improved in recent years. However, as life expectancy and population increased, the number of stroke survivors increased [1], with 85 percent of survivors requiring only partial rehabilitation due to hemiplegia [2]. Patient recovery by rehabilitating which involves repeating the same exercise in the same posture is significant for restoring the motor function that controls movement and enhancing muscular strength. Traditional physical therapy necessitates the services of a physical therapist, which takes time, and requires the expertise of a physical therapist. In addition, there are too many patients for the number of physical therapists available. Many patients will have to wait for treatment, although immediate rehabilitation may be effective more [3]. To find solutions to these issues, several robots have been developed specifically to assist in rehabilitation. The authors have developed various types of rehabilitation robots especially the upper limb [4], [5]. The physiotherapy robot has several distinguishing features, including high repetition efficiency, changing the level of assistance based on the patient's strength, and the ability to accurately measure and store patient data to assess the patient's physical condition, etc. [6]. Physical therapy robots can assist physical therapists in reducing their workload and make it possible to provide better care for patients. In addition, rehabilitation gamification and a colorful simulation environment, that make patients have more motivation and involvement in their recovery, can be added.

Physiotherapy robots for the upper limb can be divided into two categories: Exoskeleton and end-effector physiotherapy robots [6], [7]. The structure of wearable exoskeleton-type robots corresponds to the structure of the patient body. This allows a patient to better control the movement of each joint or part of a patient's body than with the end-effector type. However, the length of the robot arm must be adjusted for each user. The majority of these robots have a large and complex structure. Consequently, the cost and inertia values are both high. The amount of inertia affects the robot's movement fluidity. The ARMin III [8], and the CUREs robot [4] are examples of exoskeletons. The CUREs robots have been developed based on compact size, ease of relocation, ease of use, flexible training, and safety. The end-effector physiotherapy robot, on the other hand, has only one point of contact with the user, such as the wrist, forearm, or upper arm. As a result, the structure of this type of robot is very simple and supports a diverse group of users. It is also suitable for natural movements or movements that are used in everyday life (Activity of Daily Living: ADLs). The end-effector type examples include MIT-Manus [9], GENTLE/s [10], PASCAL [11], and EMU [12].

Robot training can be categorized into passive mode, active mode, active-assist mode, active-resist mode, and bimanual exercise [7], [13], [14]. Each mode is selected according to the patient's performance. The operating modes of each robot may apply the different control strategies [15], [16]. The exercises can be repetitive movements in a specific direction and have no functional purpose; on the other hand, some exercises are aimed at stimulating functional motor tasks, for example, picking up an object.

In recent years, many control strategies was developed for functional training, especially impedance-based assistance strategies. These strategies are based on the concept of "assist-as-needed" because when the patient deviates from the predefined path, the assistance forces increase. Some impedance-based assistance strategies are PD controller or virtual tunnel that behaves as a spring-damper [15]. Their clinical effectiveness was reviewed in several studies [17], [18], [19]. Moreover, some strategies have more functions by interacting with the real object [20] or a Virtual Reality environment [17], [21].

To focus on developing a rehabilitation robot for physical functional training, the 3D end-effector type robot and the spring-damper virtual wall strategy, also known as the virtual tunnel, with gravity compensation are chosen for active mode. The patient is allowed to freely move along the path and is restricted from moving out. This is the initial step toward developing further therapeutic modalities.

A 3D end-effector base on a five-bar linkage has been proposed to improve the common end-effector type that covers mechanical design, dynamic control strategy, and application of rehabilitation training or exercise. The dynamic controllers are deweighting with gravity compensation, passive mobilization or active assistive, and the virtual spring-damper wall concept. These controllers are used for developing functional rehabilitation training or exercise from an engineering point of view based on experiences in developing various types of rehabilitation robots. The experiments, based on the performance of the controllers, have been conducted with healthy subjects. The experimental results have shown very promising results and can be extended to various types of functional rehabilitation.

2. 3D End-Effector Robot

2.1. Structure

The 3DEE robot (3D end-effector robot) is an end-effector upper-limb rehabilitation robot that attaches to the wrist. This robot was designed to study the possibilities of rehabilitation and to be developed for activities of daily living (ADLs) training. The structure of the 3DEE robot is a 3-dimensional five-bar linkage manipulator (3 DOF), as shown in Fig. 1 The first motor

at the base is responsible for making the robot rotate about a vertical axis. The second and the third motors drive the five-bar linkage mechanism. The designed motors' location allows the robot arm to have a lower moment of inertia than a robot with motors on the arm. In addition, motors are connected to cable transmission. At the end-effector, a lightweight 3-axis-force sensor is mounted between the end of the robot arm and the spline with a freely-rotate universal joint.

A robot with link lengths of 0.6 m. and 0.6 m. can operate in a workspace of approximately 1 m. x 0.65 m. x 0.6 m. A range of motion is shown in Table 1. The robot's location can be set in 2 alternative positions: front position and side position. First, as shown in Fig. 2(a), the robot is in front of the user. Second, as shown in Fig. 2(b), the robot is on the user's side, either left or right, and the screen is optional. Both setups can be applied to the training with objects placed on a table.

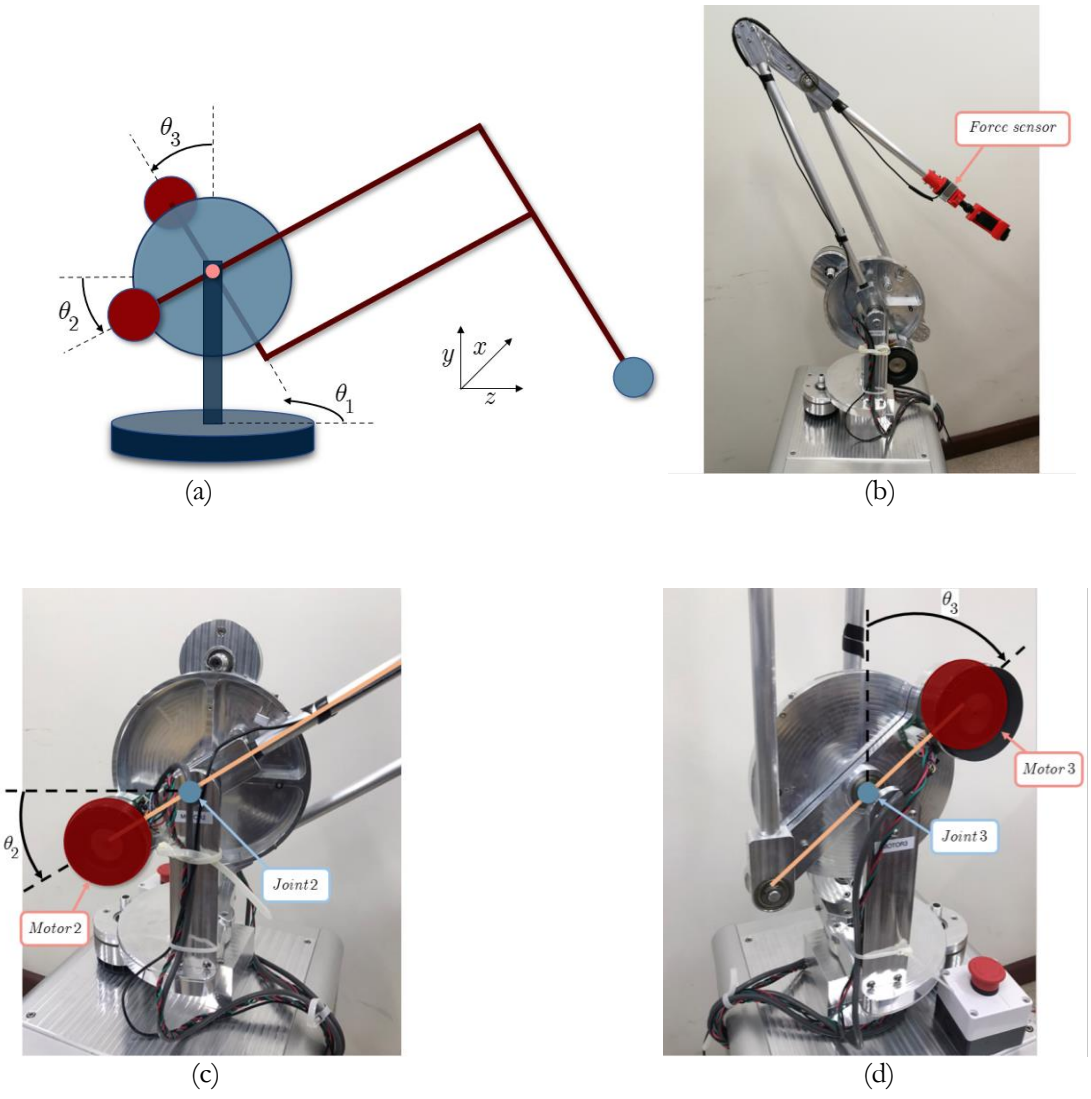

Fig. 1. (a) Schematic of the 3DEE robot, the y-axis points upward, the z-axis is approach direction, and the x-axis is due to the right-hand rule, (b) the 3DEE robot with an external force sensor, (c) the motor 2 attached to a driven link of the five-base with a distance from the rotation joint 2, and (d) Similarly to the motor 2, the motor 3 attached to another driven link. The orange lines in the last two figures represent the robot's links.

DOI:10.4186/ej.2022.26.11.29

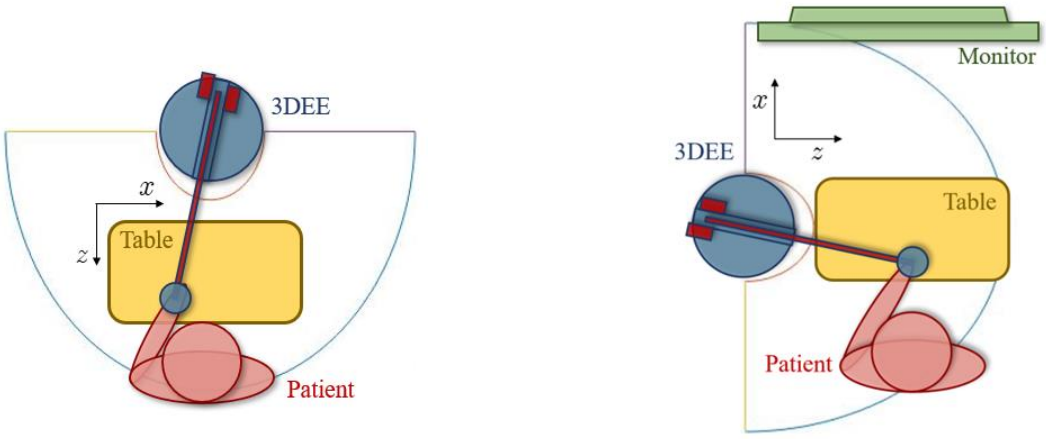

(a) (b)

Fig. 2. The robotics installation with the table (a) Front position (b) Side position.

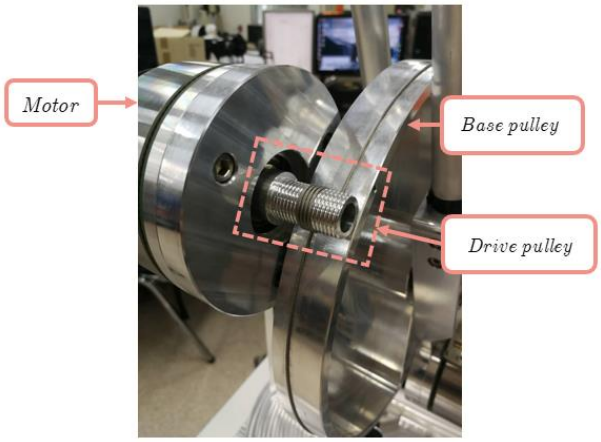

Fig. 3. Cable transmission.

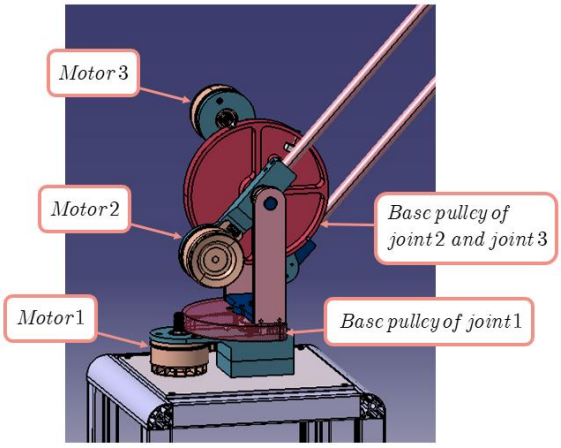

Fig. 4. Motor configuration.

Table 1. Range of motion. (Unit is degree).

	Joint 1	Joint 2	Joint 3
Range of motion	180	100	95
From	-90	10	-23
To	90	110	72

2.2. Power Transmission

The 3 DC brushless 600W motors are connected to a cable transmission system (capstan transmission system) as shown in Fig. 3, which has low backlash, low friction, no lubrication, compact transmission, and good backdrivability [4], [22]. Figure 3 shows the drive pulley attaches to the motor and the cable from the base pulley runs through the groove of the drive pulley's thread. The gear ratio can be calculated as

$$Gear\ ratio = \frac{\phi\, base\ pulley}{\phi\, driving\ pulley} = \frac{225\, mm.}{15\, mm.} = 15 \qquad (1)$$

Figure 4 shows the configuration of the motor. Motor 1 is fixed and the base pulley is the part rotating about the vertical axis. On the other hand, because joint 2 and joint 3 are on the same axis, the other motors are designed to drive the links on the same fixed base pulley, facing in the opposite direction, and using the same cable. This configuration has the benefit of compactness. Moreover, the transmission design, "the grooved drive pulley and the clean base pulley", gives the high capability as well as ease of robot assembly [22].

2.3. Gravity Compensation Configuration

For the robot configuration, as shown in Fig. 4, motors 2 and 3 are located next to the robot joints and used as counterweights to reduce the moment of inertia, due to the link mass, appearing at the driven joints of the five-bar linkage by shifting the center of mass of the driven links close to the joints as shown in Fig. 1(c) and 1(d). So, the workload on the motors can be reduced as a result, smaller motors can be selected. The 3DEE software, developed based on the gravity compensation technique as described in section 3.2, is used to compensate for the unexact counterbalance between link weight and motor weight. The gravity compensation control to balance the link weight plus unknown external loads is also described. The unknown external load is

based on a human arm reacting to the end-effector of the robot. This gravity compensation control for unknown external loads will be used for some of the training activities.

2.4. Safety

The safety of the robot system is considered for both hardware and software. In terms of hardware, the mechanical limit restricts the robot from moving beyond the desired operating space. The motion control software is developed based on stable dynamic control algorithms. The stability of the controller is also directly related to dynamics safety [23]. The torque limit and watchdog for some abruption changes of speeds and forces produced in control loops are implemented to ensure the safety of users. In addition, the robot contains an emergency switch that must be released before being used. When the operator, on the other hand, notices a risk, the emergency stop button can be used to bring the robot to a complete stop.

3. Control Algorithms and Associated Training Activities

The dynamic control algorithms developed in this research are based on training activities used in stroke functional training. The hemiparesis patient who uses this training should not be in a severe condition. The objective of the training is aimed at upper-limb day-to-day activities, such as moving an object on a table, inserting an object into a hole, stacking objects, etc. The dynamic control algorithms are developed based on the flexibility in the interaction of the robot. The training activities used for developing the controller are as follows:

- **Deweighting with Gravity Compensation techniques** by applying an upwards force and the patient's arm can move freely in a horizontal plane.
- **Passive Mobilization** is where the active assistive force will be applied to the patient's arm along a predefined trajectory. The predefined trajectory can be in the direction of the forearm.
- **Virtual Spring-Damper Wall** is where the patient's arm is restricted within a predefined path as a spring-damper cylindrical virtual wall tube or a tunnel path. The robot will not assist a patient's arm along the path.

3.1. Dynamic Model

The dynamic model represents the correlation between motion and physical factors such as mass and force. According to Siciliano et al., 2009 [24], the joint space dynamic model is described by

$$B(\theta)\ddot{\theta} + C(\theta,\dot{\theta})\dot{\theta} + F_v\dot{\theta} + F_s\,\mathrm{sgn}(\dot{\theta}) + G(\theta) = \tau \qquad (2)$$

where θ is a joint angular position, $B(\theta)\ddot{\theta}$ is the inertial torque matrix, $C(\theta,\dot{\theta})\dot{\theta}$ represents the centrifugal effect and the Coriolis effect, $F_v\dot{\theta}$ is the viscous friction torque matrix, $F_s\,\mathrm{sgn}(\dot{\theta})$ is the Coulomb friction torque matrix, $G(\theta)$ is the gravitational torque matrix, τ is the input torque matrix.

3.2. Gravity Compensation

The gravity term $G(\theta)$ in Eq. (2) is used in the gravity compensation control. This is to eliminate an unbalance due to the offset between the center of gravity of a link and the center of rotation of the joint. In Eq. (3), the term τ_G, the torque generated by the motor, is set equal to $G(\theta)$. The system dynamics with gravity compensation can be written as

$$B(\theta)\ddot{\theta} + C(\theta,\dot{\theta})\dot{\theta} + F_v\dot{\theta} + F_s\,\mathrm{sgn}(\dot{\theta}) + G(\theta) = \tau_G - \tau_{External} \qquad (3)$$

where $\tau_{External} = J^T(\theta)h_e$, $J^T(\theta)$ is the Jacobian transpose term of the manipulator arm, and h_e is the external force applied at the end-effector by a patient.

By assuming that the gravity term can be obtained from the very accurate dynamic model Eq. (3) and $G(\theta) = \tau_G$, the dynamic model of the manipulator becomes

$$B(\theta)\ddot{\theta} + C(\theta,\dot{\theta})\dot{\theta} + F_v\dot{\theta} + F_s\,\mathrm{sgn}(\dot{\theta}) = -\tau_{External} \qquad (4)$$

Equation (4) shows that if the robot arm has no external force, $\tau_{External} = 0$, the robot arm will be in balanced mode.

Deweighting with Gravity Compensation

To eliminate the gravitational effect of the robot arm and the unknown external loads at a robot end-effector, a patient arm mass, and force applied by a patient. The deweighting with gravity compensation is proposed, as shown in Fig. 5. The feedback gravity torque (τ_G) is provided by the gravity compensation term by assigning that

$$\tau_G = G(\theta) \qquad (5)$$

Deweighting uses the external force measured by a force sensor as $h_e = \begin{bmatrix} h_x & h_y & h_z \end{bmatrix}^T$. Only the y-axis or gravity direction is used. Therefore, the external force used in the deweighting with gravity compensation control is

DOI:10.4186/ej.2022.26.11.29

$$F_y = \begin{bmatrix} 0 & h_y & 0 \end{bmatrix}^T \tag{6}$$

To reduce the effect of a rapid change of an external force measured from the force sensor, some viscous damping is added to the external force as

$$F_E = -F_y(1 + \text{sgn}(F_y)K_v\dot{x}) \tag{7}$$

where K_v is a velocity gain and $\dot{x}$ is the end-effector velocity. The $\text{sgn}(\cdot)$ is the sign function. And the external torque can be written as

$$\tau_E = J(\theta)^T F_E \tag{8}$$

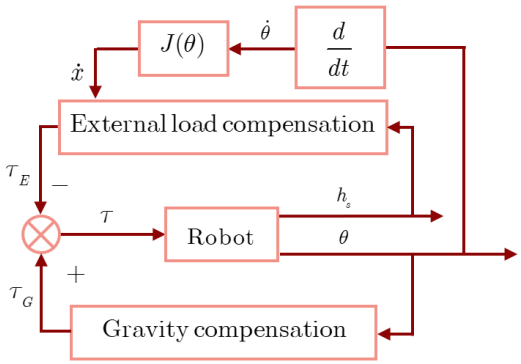

Fig. 5. Block diagram of the deweighting with gravity compensation.

3.3. Passive Mobilization

The control strategy for this training is the combination of motion control and force control or the active assistive control. The block diagram of this control strategy is shown in Fig. 6. There are two loops, the inner loop is a velocity control loop while the outer loop is a force control loop. The impedance control is used to define the relationship between the driving torque and the angular position of the joint. In the control loop, the actual motor torques can be estimated from the measurement of the motor current. The detail of this controller can be found in the upper-limb exoskeleton robot (CUREs) [4]. The desired torque $T_{L,d}$ can be obtained by a simple stiffness P and the angular error between the desired angle, θ_d, and the actual angle, θ_L, as

$$T_{L,d} = P(\theta_d - \theta_L) \tag{9}$$

However, when the angular position error, between the desired path and actual position, increases, a higher helping force is needed to guide the movement of the patient's arm with minimal force. For small angular position error, the helping force is adjusted by using the virtual wall control strategy as described in [4] as

$$T_{L,d} = \text{sgn}\left|\theta_d - \theta_L\right| K_p \; e^{\left|\theta_d - \theta_L\right| K_f} - 1 \tag{10}$$

where K_p and K_f are the gains of the impedance part that can be adjusted to obtain a suitable desired torque of the outer loop control, which is the torque control loop, as shown in Fig 6. The detail of obtaining K_p and K_f are described in [4].

3.4. Virtual Spring-Damper Wall Strategy

This control system was developed for patients with muscle weakness from Brunnstrom stage 3 onwards according to the Medical Research Council (MRC) criteria for active mode training. Brunnstrom stage 3 is the stage to which the patient's muscle contraction becomes controllable, or the patient is able to move spontaneously without compensating for gravity. Therefore, the virtual spring-damper wall strategy, also known as the Tunneling Strategy [10], [15], [21], [25], is implemented to restrict the user to move along a path but the resist and assist forces are not provided along the path. This control system operates in the same way as a spring-damping tunnel or a cylindrical wall along the pre-defined path which is defined as the axis of the cylindrical wall as shown in Fig. 7. This virtual cylindrical wall will not allow the end-effector of the robot to go beyond this wall. The wall will generate an opposite force in the orthogonal direction to the wall when the end-effector tries to move beyond the wall. This control system also includes a speed-resisting damper that can move comfortably without resistance in the direction of the predefined path and the gravity compensation that can remove the effect of the robot arm's weight. The block diagram of this control strategy is shown in Fig. 8.

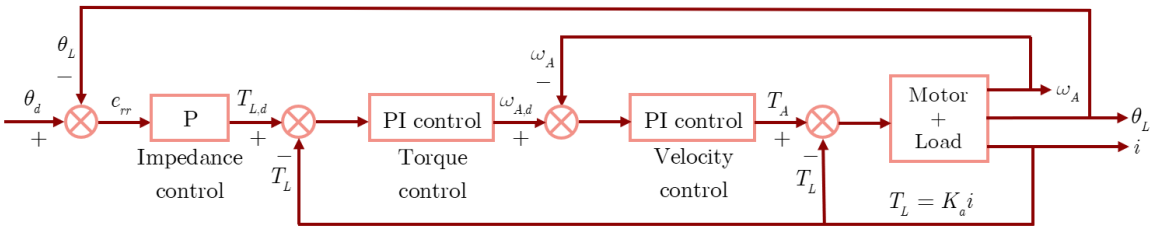

Fig. 6. Block diagram of the active assistive control strategy [4].

The virtual wall model can be divided into two main terms: spring term and damping term. The spring force (F_s) can be obtained as

$$F_s = k\,D(\Delta x) \tag{11}$$

where $D()$ is the deadband function implemented to reduce spring force redirection-induced volatility around zero and to be a spring-force-free area for freely moving, k is spring constant, and

$$\Delta x = x_{nearest} - x \tag{12}$$

is the deviation between the end-effector position (x) to the nearest position on the path ($x_{nearest}$). (Orthogonal vector to the path of motion) The deadband function with the width of the deadband (a) can be written as follows:

$$D(\Delta x) = \begin{cases} \Delta x - a & \Delta x > a \\ 0 & -a \le \Delta x \le a \\ \Delta x + a & \Delta x < -a \end{cases} \tag{13}$$

For the damping term, the damping force (F_d) can be evaluated from the following equation.

$$F_d = -c\dot{x}_n \tag{14}$$

where c is the damping coefficient, and $\dot{x}_n$ is the end-effector velocity in the X, Y, and Z axes perpendicular to the path, as obtained from the end-effector velocity ($\dot{x}$) minus the velocity parallel to the line of the path ($\dot{x}_p$) as indicated in Eq. (15).

$$\dot{x}_n = \dot{x} - \dot{x}_p \tag{15}$$

The force that the robot arm exerts on the human arm due to the virtual wall (F_w) is

$$F_w = F_s + F_d \tag{16}$$

And the torque due to the virtual wall (τ_w) can be written in the following equation:

$$\tau_w = J^T(\theta)F_w \tag{17}$$

leads to the controlled input torque

$$\tau = J^T(\theta)(k\,D(\Delta x) - c\dot{x}_n) + G(\theta) \tag{18}$$

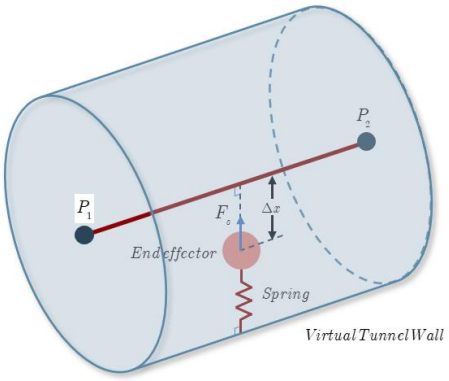

Fig. 7. Interaction of Spring virtual wall model on the end-effector. Pink circles represent the end-effector, the red lines represent the predefined path between the initial point (P_1) and the second point (P_2), and blue arrows represent the restrict force exerted by the robot.

To ensure the stability of the proposed control strategy, the Lyapunov function is used in the form as

$$V(\theta,\Delta x) = \frac{1}{2}\dot{\theta}^T B(\theta)\dot{\theta} + \frac{1}{2}D(\Delta x)^T kD(\Delta x) \ge 0,\ \ \forall\theta, \Delta x \ne 0 \tag{19}$$

where k is a symmetric positive definite matrix, and the derivative of Eq. (19) is

$$\dot{V} = \dot{\theta}^T B(\theta)\ddot{\theta} + \frac{1}{2}\dot{\theta}^T \dot{B}(\theta)\dot{\theta} + D(\Delta\dot{x})^T kD(\Delta x) \tag{20}$$

Since $\dot{x}_{nearest} = 0$,

$$\Delta\dot{x} = -J(\theta)\dot{\theta} \tag{21}$$

Substituting Eq. (2), Eq. (18), and Eq. (21) into Eq. (20) gives

$$\begin{aligned} \dot{V} &= \dot{\theta}^T(-C(\theta,\dot{\theta})\dot{\theta} - F_v\dot{\theta} - F_s\,\mathrm{sgn}(\dot{\theta}) - G(\theta) + \tau) + \frac{1}{2}\dot{\theta}^T\dot{B}(\theta)\dot{\theta} \\ &\quad - J^T(\theta)\dot{\theta}^T kD(\Delta x) \\ &= \frac{1}{2}\dot{\theta}^T(\dot{B}(\theta) - 2 - C(\theta,\dot{\theta}))\dot{\theta} - \dot{\theta}^T(F_v\dot{\theta} - F_s\,\mathrm{sgn}(\dot{\theta})) + (\dot{\theta}^T\tau - \dot{\theta}^T G(\theta) \\ &\quad - J^T(\theta)\dot{\theta}^T kD(\Delta x)) \\ &= -\dot{\theta}^T F_v\dot{\theta} - \dot{\theta}^T F_s\,\mathrm{sgn}(\dot{\theta}) - \dot{\theta}^T c\dot{x}_n \le 0 \end{aligned} \tag{22}$$

where $\dot{B}(\theta) - 2C(\theta,\dot{\theta})$ is skew-symmetric. From the Eq. (22), $\dot{V} = 0$ only if $\dot{\theta} = 0$. At the equilibrium point ($\dot{\theta} = 0, \ddot{\theta} = 0$), Eq. (2) combined with Eq. (18) becomes

$$k\,D(\Delta x) = 0 \tag{23}$$

then Eq. (12) can be simplified to

$$x_{nearest} - x = 0 \tag{24}$$

DOI:10.4186/ej.2022.26.11.29

From the above equations, the $x = x_{nearest}$ is the largest invariant set in the set where $\dot{V} = 0$. Using the Invariant Set theorem of La Salle, globally asymptotically stable can be concluded.

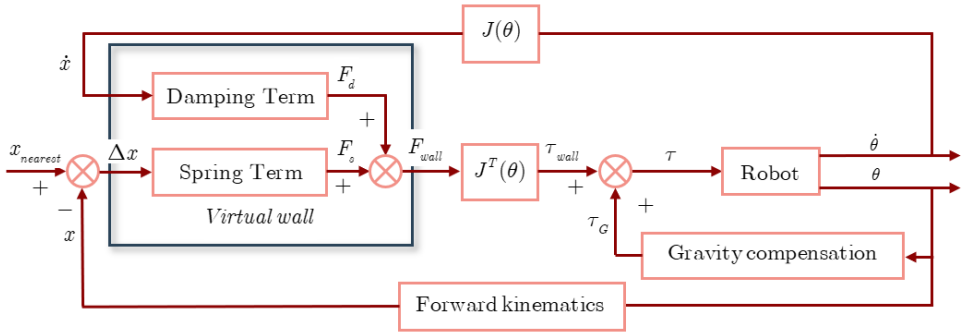

Fig. 8. Block diagram of the virtual spring-damper wall strategy.

4. Modes of Training

In the previous section, the control strategies and the associated training activities have been described. The training activities as Deweighting with Gravity Compensation, Passive Mobilization, and Virtual Spring-Damper Wall. The exercises using the deweighting with gravity compensation are straightforward. The robot is to hold the patient's arm at a certain level and the patient arm is free to move in the horizontal plane.

The exercise with Passive mobilization is similar to the active assistive control strategy as described in Section 3.3 and [4]. The predefined path can be obtained by moving the patient's arm along the desired path following the medical recommendation. The desired path can be captured through the encoders of the robot or using a stereovision camera of the robot. The detail of the training using the active assistive is developed by the authors and described in detail in [4].

In this section, the detail of the training using the Virtual Tunnel or the Cylindrical Virtual wall, based on Section 3.4, will be described with a specific training pattern as the 3D eight-point pattern.

4.1. Virtual Tunnel or Cylindrical Wall Training Mode

Training or exercising using the Virtual Cylindrical Wall or the Virtual Tunnel is based on the controller described in Section 3.4. The virtual wall of the cylindrical tube is modeled as a virtual spring and damper. A cylindrical tube is defined as the desired path for training. A physiotherapist can reprogram or alter the position of the patient's wrist, known as the end-point position of the robot arm, or choose from a pre-programmed trajectory. In the custom trajectory option, a physiotherapist arranges the patient's posture and records the end-effector positions of the robot held by the patient. The user must move from the start point to the target point of the desired path along the sub-path created from each consecutive point of the desired path. For the 3D eight-point pattern as shown in Fig. 9, the 8 points are located on the same horizontal plane with equal angles and equal distance from the center point. The patient will guide the end-effector of the robot to a target point and back to the center point before moving to the next target which is randomly generated or generated counterclockwise sequence as shown in Fig. 9.

4.2. Dashboard and Program Interface

Figure 10 shows four main components of the dashboard display: graphical data display of robot driving torque and human torque, data display, graphical display of robot end-point motion and human hand motion, and control panel. The robot data and the data collected from the user can be selected to be displayed in the graphical data display and the data display sections. The graphical display section presents the path (lines between circles), specified positions (pink circle), the target position (dark gray circle), the actual end-effector position (blue circle), and the 3D scene (plane with grid). Additionally, the 3D view can be rotated for a better viewing angle. The buttons for the operations section, path options, and the controller's gain adjuster are in the control panel area.

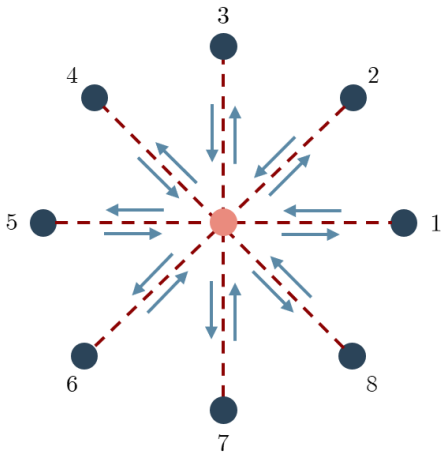

Fig. 9. The 8-points pattern of the virtual tunnel program. The blue points represent the targets, the pink point represents the center point, the red dash lines represent the path, and the blue arrows represent the direction of the movement.

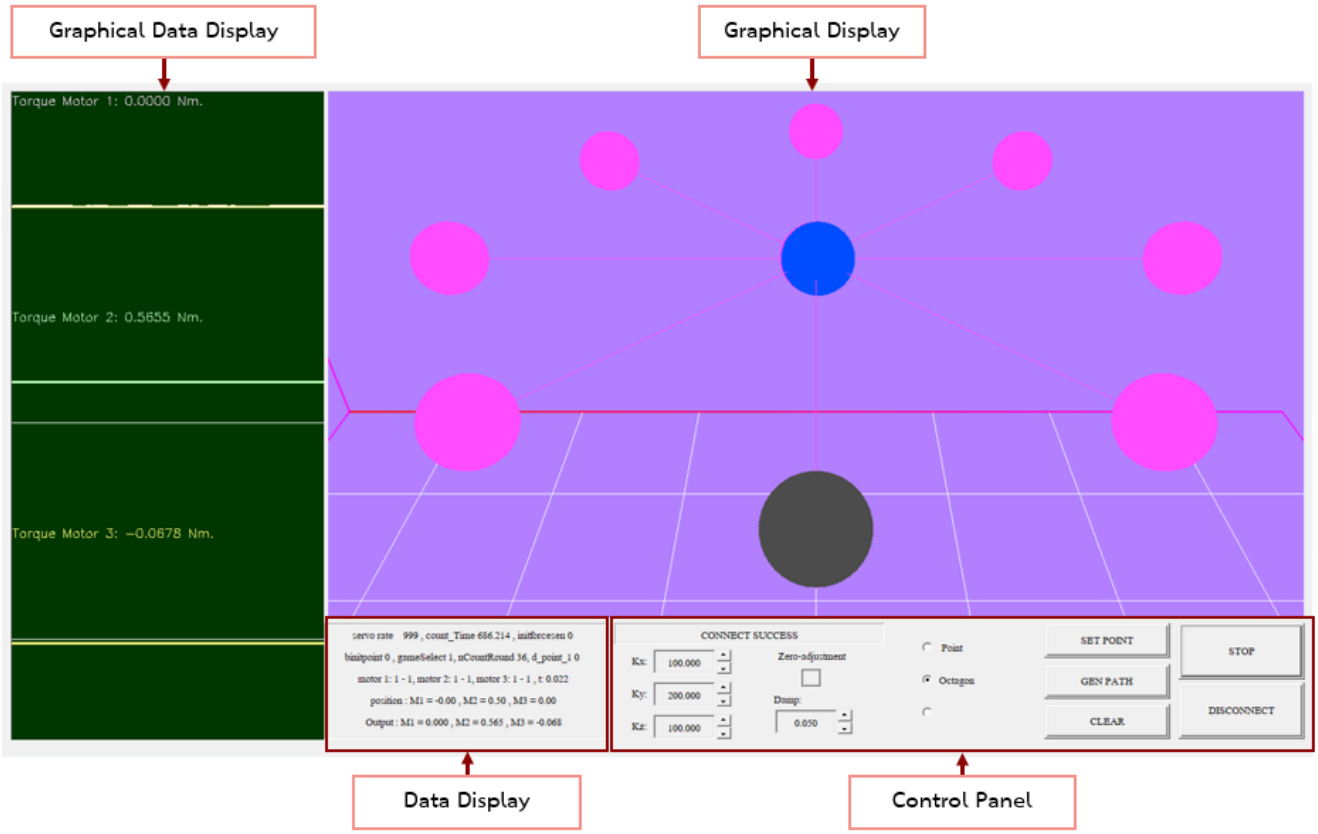

Fig. 10. Program interface of virtual tunnel program.

5. Experiment and Experimental Results

5.1. Gravity compensation

Gravity compensation, described in section 3.2, is a crucial component of the 3DEE robot's control strategies. As a result, before testing the control system, the accuracy of the gravity compensation of the robot arm must be verified first. In the case of without external force and zero initial condition, the robot can remain stationary regardless of the position of the robot arm. The end-effector of the robot arm, to which a human hand is attached, can be moved freely in the horizontal plane while the vertical motion can be set by the gravity compensation without a force sensor. If a more precise vertical position needs to be maintained, the force sensor information can be included in the controller. This procedure is to verify the gravity compensation for an unknown external load or a human armload. Fig. 11 shows the x-y-z position of the end-point of the robot arm. No external load is applied during the first 1.5 seconds, the graph shows that the robot end-point is maintained at its original position, especially vertical position. Then an external unknown load or a human arm with force is attached to the end-effector of the robot, from the graph in Fig. 11(a), it is shown that the vertical position is maintained its vertical position or y-axis. Fig. 11(b) shows an unknown force applied at the end-effector of the robot. When the arm is detached from the robot, the robot is maintained its position, and the force at the end-effector is back to the original state.

5.2. Virtual Spring-Damper Wall Strategy

To verify the effectiveness of the virtual spring-damper wall strategy in the training or exercise with the virtual tunnel, the experiments are conducted on healthy subjects. The 3DEE robot can be located in front of or on a side of the subject as shown in Fig. 2(b). The monitor is placed in front of the subject. And a predefined path is set on the Z-axis between point 1 [0, 0.50, -0.15] and point 2 [0, 0.50, 0.15] to make the controller's performance more prominent. Because of the virtual wall, the subject can freely move along the z-axis or axis of the cylindrical virtual wall. When the subject tries to move away from the z-axis against the virtual wall, there will be a force, from the virtual wall, that pushes the subject back to the virtual wall axis, as shown in Fig. 12. The detail of position, the deviation from the reference path, and interaction force in each axis are shown in Fig. 13. If there is an unknown external force applied to the robot end-effector, the controller will create the interaction force to maintain the motion of the end-effector within the volume of the cylindrical virtual wall. The experiment is closed to the practical functional training, where the subject normally moves gradually or slowly in the direction of a path or predefined path with carrying an object. The virtual wall parameters can be adjusted. In this experiment, the spring constant, the deadband, and the damping coefficient, as shown in Fig. 6, are set as $k = \begin{bmatrix} 200 & 500 & 200 \end{bmatrix} \mathrm{N/m}$, $a = 10mm.$, $c = 0.5Ns/m^2$,

respectively. In the experiment, the actual end-effector position, the deviation (Δx) from Eq. (12), and the interaction force are recorded. The interaction force between the human hand or the subject and the robot is measured by a force sensor. The well-known 3D 8-point pattern, as predefined paths, has been tested in the work as well. As shown in Fig. 14, the center point of the pattern is at [0, 0.50, 0]. There are nine target points including the center point. The target points circle around the center point. The distance between the targets and the center point is 160 mm. The predefined paths of the 8-point are shown in Fig. 9. Figure 14 shows the experimental results of the 8-point pattern. Each path is implemented with a virtual wall. The end-effector can be moved freely in the direction from the center point to each target point. The result demonstrates that the subject can proceed along with the pattern with minor deviations. This mode of training can be applied to functional rehabilitation. By the way, the controller algorithm as described in section 3.3 or passive mobilization can be applied in the z-direction as well to provide active assistive force to help the subject to move in the z-direction whenever needed. This is another mode of training.

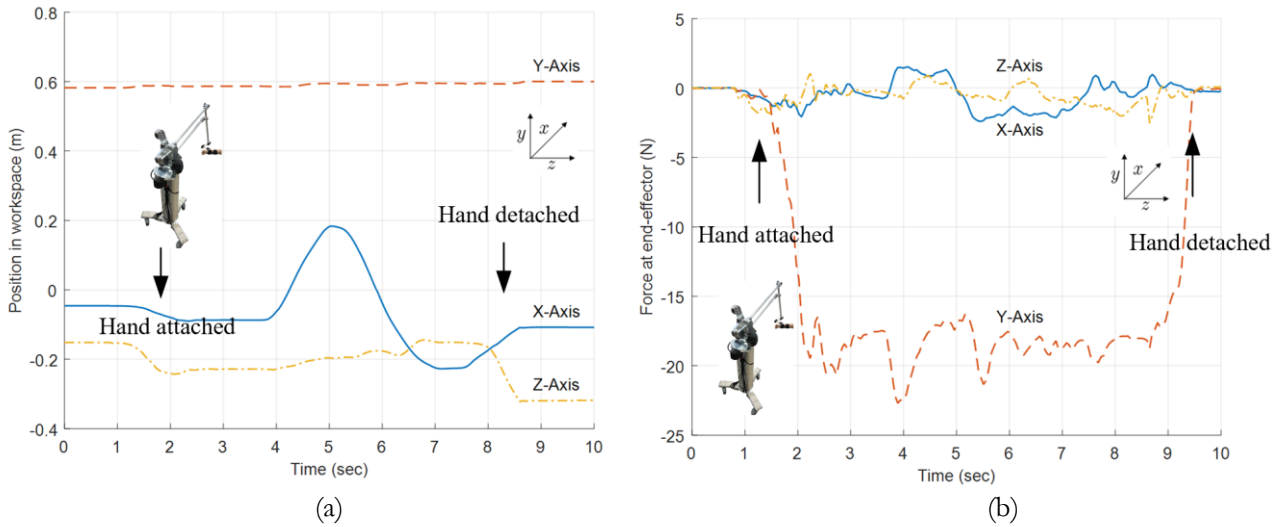

(a) (b)

Fig. 11. (a) The end-effector position, and (b) the end-effector force in Cartesian space for the Gravity compensation with unknown external force.

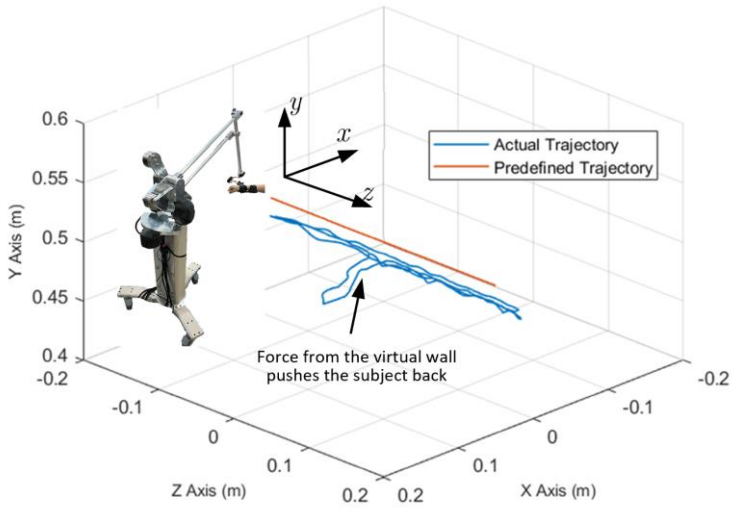

Fig. 12. The actual and predefined trajectory (z-axis) of the robot's end-effector.

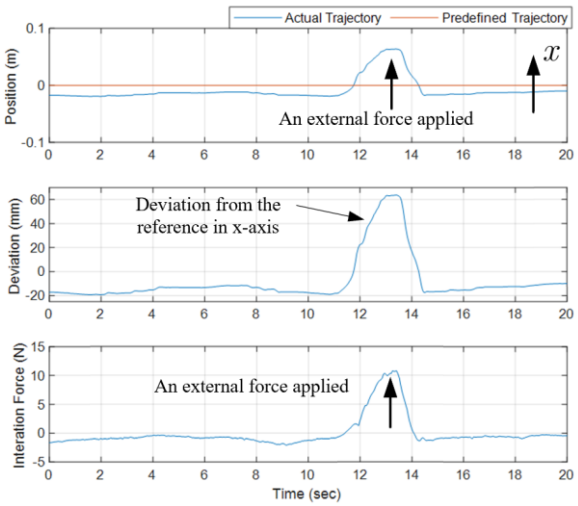

(a)

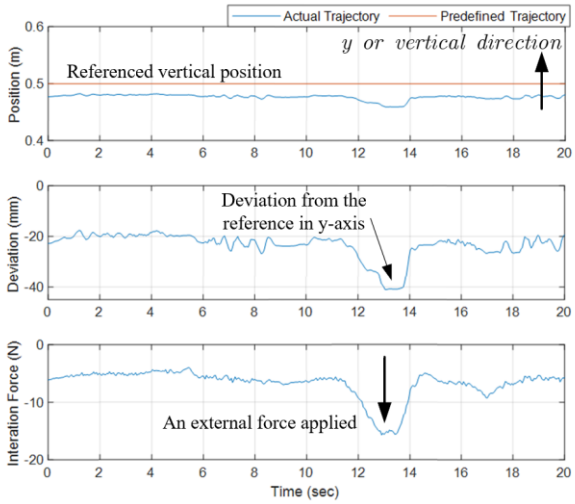

(b)

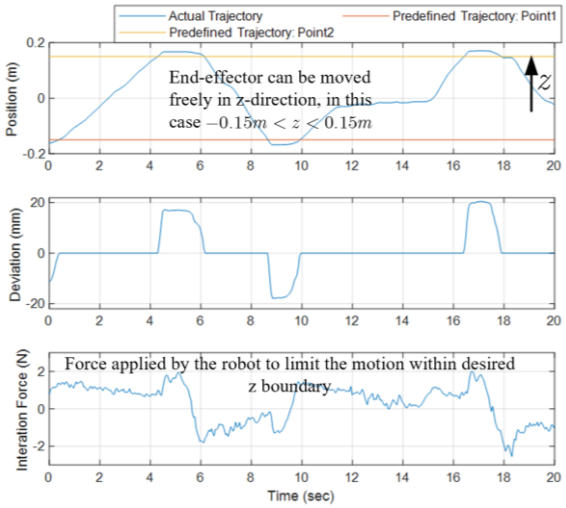

(c)

Fig. 13. The recorded data from the experiment (a) in X axis, (b) in Y axis, and (c) in Z axis. The first of each graph represents the actual and the predefined trajectories of the robot's end-effector attached to the subjects' wrist. The second and the third represent the deviation (Δx) from Eq. (12) and the measured interaction force.

DOI:10.4186/ej.2022.26.11.29

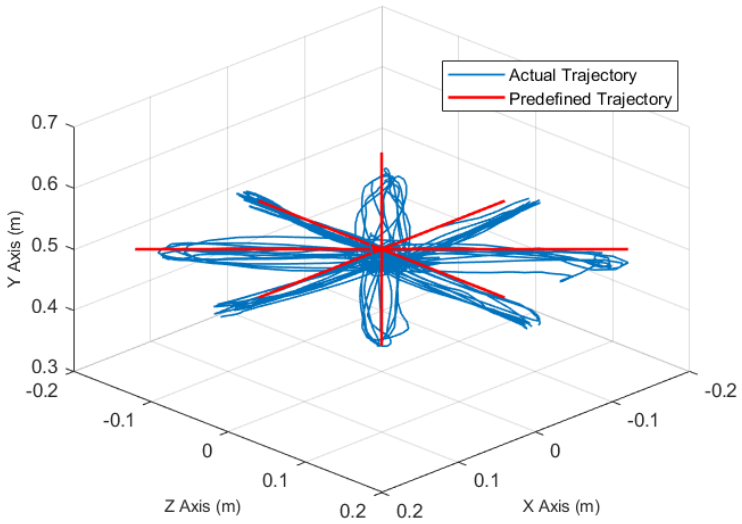

Fig. 14. The actual and predefined trajectory of the robot's end-effector in the 8-points pattern test.

6. Conclusion

In this paper, the development of the 3D end-effector robot is described in both dynamics model, controller, hardware, and software. The experiments demonstrate the first-step success of the useful programs for stroke rehabilitation, especially functional rehabilitation: the high accuracy of the gravity compensation with an unknown load controller, the passive mobilization, and the more efficiency of the virtual spring-damper wall strategy for active movement training. The experiments show that the robot configuration and the controllers are very promising for the functional rehabilitation of hemiparesis patients who suffered from stroke. The training programs can be developed based on the controllers developed in this paper. Some of the training or exercising has demonstrated the effectiveness of the controllers. And the robot is ready for a clinical trial.

Acknowledgement

Part of this project is funded by National Research Council of Thailand (NRCT).

References

[1] V. L. Feigin *et al.*, "Global, regional, and national burden of neurological disorders, 1990-2016: A systematic analysis for the Global Burden of Disease Study 2016," *The Lancet Neurology,* vol. 18, no. 5, pp. 459-480, 2019.

[2] T. Truelsen, B. Piechowski-Jóźwiak, R. Bonita, C. Mathers, J. Bogousslavsky, and G. Boysen, "Stroke incidence and prevalence in Europe: A review of available data," *Eur J Neurol,* vol. 13, no. 6, pp. 581-98, Jun 2006.

[3] X. Wu, P. Guarino, A. C. Lo, P. Peduzzi, and M. Wininger, "Long-term effectiveness of intensive therapy in chronic stroke," *Neurorehabil Neural Repair,* vol. 30, no. 6, pp. 583-90, Jul. 2016.

[4] A. Sutapun and V. Sangveraphunsiri, "A novel design and implementation of a 4-DOF upper limb exoskeleton for stroke rehabilitation with active assistive control strategy," *Engineering Journal*, vol. 21, no. 7, pp. 275-291, Dec. 2017.

[5] T. Eiammanussakul and V. Sangveraphunsiri, "Mechanical power to identify human performance for a lower limb rehabilitation robot," *Engineering Journal,* vol. 23, pp. 91-105, Aug. 2019.

[6] L. M. Weber and J. Stein, "The use of robots in stroke rehabilitation: A narrative review," *NeuroRehabilitation,* vol. 43, no. 1, pp. 99-110, 2018.

[7] M. Babaiasl, S. H. Mahdioun, P. Jaryani, and M. Yazdani, "A review of technological and clinical aspects of robot-aided rehabilitation of upper-extremity after stroke," *Disabil Rehabil Assist Technol,* vol. 11, no. 4, pp. 263-80, 2016.

[8] T. Nef, M. Guidali, and R. Riener, "ARMin III – Arm Therapy Exoskeleton with an Ergonomic Shoulder Actuation," *Applied Bionics and Biomechanics,* vol. 6, no. 2, pp. 127-142, 2009.

[9] H. I. Krebs, N. Hogan, M. L. Aisen, and B. T. Volpe, "Robot-aided neurorehabilitation," *IEEE Transactions on Rehabilitation Engineering,* vol. 6, no. 1, pp. 75-87, 1998.

[10] R. Loureiro, F. Amirabdollahian, M. Topping, B. Driessen, and W. Harwin, "Upper limb robot mediated stroke therapy—GENTLE/s approach," *Autonomous Robots,* vol. 15, no. 1, pp. 35-51, 2003.

[11] A. Koenig, U. Keller, K. Pfluger, A. Meyer-Heim, and R. Riener, "PASCAL: Pediatric arm support robot for combined arm and leg training," in *2012 4th IEEE RAS & EMBS International Conference on Biomedical Robotics and Biomechatronics (BioRob)*, 2012, pp. 1862-1868.

[12] J. Fong, V. Crocher, Y. Tan, D. Oetomo, and I. Mareels, "EMU: A transparent 3D robotic

manipulandum for upper-limb rehabilitation," in *2017 International Conference on Rehabilitation Robotics (ICORR)*, 2017, pp. 771-776.
[13] R. M. Mahoney, H. F. M. Van der Loos, P. S. Lum, and C. Burgar, "Robotic stroke therapy assistant," *Robotica,* vol. 21, no. 1, pp. 33-44, 2003.
[14] P. Poli, G. Morone, G. Rosati, and S. Masiero, "Robotic technologies and rehabilitation: new tools for stroke patients' therapy," *Biomed Res Int,* vol. 2013, 2013.
[15] L. Marchal-Crespo and D. J. Reinkensmeyer, "Review of control strategies for robotic movement training after neurologic injury," *Journal of NeuroEngineering and Rehabilitation,* vol. 6, no. 1, p. 20, Jun. 2009.
[16] W. Meng, Q. Liu, Z. Zhou, Q. Ai, B. Sheng, and S. Xie, "Recent development of mechanisms and control strategies for robot-assisted lower limb rehabilitation," *Mechatronics,* vol. 31, pp. 132-145, Oct. 2015.
[17] A. Montagner *et al.*, "A pilot clinical study on robotic assisted rehabilitation in VR with an arm exoskeleton device," in *2007 Virtual Rehabilitation*, 2007, pp. 57-64.
[18] F. Amirabdollahian, R. Loureiro, E. Gradwell, C. Collin, W. Harwin, and G. Johnson, "Multivariate analysis of the Fugl-Meyer outcome measures assessing the effectiveness of GENTLE/S robot-mediated stroke therapy," *Journal of NeuroEngineering and Rehabilitation,* vol. 4, no. 1, p. 4, Feb. 2007.
[19] V. Klamroth-Marganska *et al.*, "Three-dimensional, task-specific robot therapy of the arm after stroke: A multicentre, parallel-group randomised trial," *Lancet Neurol,* vol. 13, no. 2, pp. 159-66, Feb. 2014.
[20] M. J. Johnson, K. J. Wisneski, J. Anderson, D. Nathan, and R. O. Smith, "Development of ADLER: The Activities of Daily Living Exercise Robot," in *The First IEEE/RAS-EMBS International Conference on Biomedical Robotics and Biomechatronics*, 2006, pp. 881-886.
[21] M. Guidali, A. Duschau-Wicke, S. Broggi, V. Klamroth-Marganska, T. Nef, and R. Riener, "A robotic system to train activities of daily living in a virtual environment," *Med Biol Eng Comput,* vol. 49, no. 10, pp. 1213-23, Oct 2011.
[22] Y. Lu and D. Fan, "Non-intervene cable wrapping method for precise cable drive," in *2012 International Conference on Optoelectronics and Microelectronics*, 2012, pp. 378-383.
[23] Q. Meng, Q. Xie, and H. Yu, "Upper-limb rehabilitation robot: State of the art and existing problems," in *Proceedings of the 12th International Convention on Rehabilitation Engineering and Assistive Technology*, 2018, pp. 155-158.
[24] L. S. B. Siciliano, L.Villani, and G. Oriolo, *Robotics: Modelling, Planning and Control.* London: Springer, 2009.
[25] T. Proietti, V. Crocher, A. Roby-Brami, and N. Jarrassé, "Upper-limb robotic exoskeletons for neurorehabilitation: A review on control strategies," *IEEE Reviews in Biomedical Engineering,* vol. 9, pp. 4-14, 2016.

Kewalee Asawapithulsert, photograph and biography not available at the time of publication.

Anan Sutapun, photograph and biography not available at the time of publication.

Maitai Dahlan, photograph and biography not available at the time of publication.

Viboon Sangveraphunsiri, photograph and biography not available at the time of publication.